scientific reports

Check for updates

OPEN

Synthesis of Ag/CuS doped mineral magnetite nanocomposite with improved photocatalytic activity against tetracycline and diclofenac pollutants

Roya Mohammadzadeh Kakhki✉ & Hadis Bolandhemmat

The contamination of water sources by pharmaceutical pollutants presents significant environmental and health hazards, making the development of effective photocatalytic materials crucial for their removal. This research focuses on the synthesis of a novel Ag/CuS/Fe_3O_4 nanocomposite and its photocatalytic efficiency against tetracycline (TC) and diclofenac contaminants. The nanocomposite was created through a straightforward and scalable precipitation method, integrating silver nanoparticles (AgNPs) and copper sulfide (CuS) into a magnetite framework. Various analytical techniques, including X-ray diffraction (XRD), scanning electron microscopy (SEM), Fourier transform infrared spectroscopy (FTIR),ultraviolet–visible spectrophotometry (UV–Vis) and energy-dispersive X-ray spectroscopy (EDS), were employed to characterize the structural and morphological properties of the synthesized material. The photocatalytic activity was tested by degrading tetracycline and diclofenac under visible light. Results indicated a marked improvement in the photocatalytic performance of the Ag/CuS/Fe_3O_4 nanocomposite (98%photodegradation of TC 60 ppm in 30 min) compared to both pure magnetite and CuS/Fe_3O_4. The enhanced photocatalytic efficiency is attributed to the synergistic interaction between AgNPs, CuS, and Fe_3O_4, which improves light absorption and charge separation, thereby increasing the generation of reactive oxygen species (ROS) and promoting the degradation of the pollutants. The rate constant *k* of photodegradation was about 0.1 min^{-1} for catalyst dosages 0.02 g. Also the effect of photocatalyst dose and concentration of TC and pH of solution was tested. The modified photocatalyst was also used for simultaneous photodegradation of TC and diclofenac successfully. This study highlights the potential of the Ag/CuS/Fe_3O_4 nanocomposite as an efficient and reusable photocatalyst for eliminating pharmaceutical pollutants from water.

Keywords Ag/CuS/Fe_3O_4 nanocomposite, Photocatalytic activity, Tetracycline, Diclofenac, Visible light

The rapid urbanization and industrialization of modern society have significantly increased contamination of groundwater, air, and fossil fuels through conventional industrial waste disposal methods[1,2]. This has led to major environmental issues like pollution and climate change, threatening ecosystems and human health[3–8]. The World Health Organization reports that environmental pollution has caused 3.7 million deaths in the twenty-first century, with 92% of the global population living in areas with severe air and water pollution[9,10]. Thus, the safe disposal of hazardous waste has become a critical priority[11–14]. Advanced Oxidation Processes (AOPs), particularly heterogeneous photocatalysis, are promising for removing organic contaminants from water and air due to their efficiency in degrading organic pollutants[15,16]. Semiconductor-based photocatalysts, especially metal oxides, are widely studied for their efficiency and cost-effectiveness in water pollution treatment[17–24]. Titanium dioxide (TiO_2) is notable for its low cost, non-toxicity, and chemical inertness but is limited to UV light activity, necessitating the development of visible-light-driven photocatalysts[25–29]. Various metal oxides, including La_2O_3, CdO, CeO_2, CaO, and ZnO, have been explored to enhance TiO_2's activity[30–32]. Incorporating magnetic nanoparticles like hematite, maghemite, magnetite, and various ferrites into photocatalysts imparts magnetic properties, allowing easy separation from solutions with a magnet[33]. These nanoparticles do not significantly

Department of Chemistry, Faculty of Sciences, University of Gonabad, Gonabad, Iran. ✉email: Romohammadzadeh@gonabad.ac.ir

affect the surface area or dispersion of the photocatalyst and can also absorb visible light, enhancing pollutant degradation[34]. One promising frontier in combating water pollution is the development of magnetic visible-light-active nanocomposites for photocatalytic environmental cleanup.

Covellite CuS, a p-type semiconductor with a narrow bandgap (1.2–2.0 eV), is notable for its low cost, non-toxicity, easy production, and excellent stability. It absorbs broad visible light, plasmon, and near-infrared (NIR) radiation, making it an effective photocatalyst[35,36]. However, its efficiency is limited by factors like morphology, size, and rapid recombination of photoexcited charges, which researchers are addressing by creating CuS-based nanoheterostructures. For example, embedding CuS nanospheres within an MCM-41 matrix has shown enhanced performance in degrading methylene blue under visible light[37]. Additionally, silver (Ag) doping enhances the photocatalytic activity of semiconductors by lowering the recombination rate of holes and electron pairs and modifying the band gap energy, making the material more active under visible light, which is particularly advantageous for wastewater treatment applications[38–40]. These advancements position CuS and Ag-doped nanocomposites as powerful photocatalysts for clean water applications.

Introducing Fe_3O_4 (magnetite) as a base material for photocatalysts adds significant functionality. Magnetite, a naturally occurring iron oxide with magnetic properties, serves as a stable and robust support for semiconductor photocatalysts like CuS[41,42]. In CuS-based nanocomposites, Fe_3O_4 provides a high surface area and facilitates the dispersion of CuS nanoparticles, enhancing reactant accessibility to catalytic sites. Additionally, Fe_3O_4's magnetic properties allow for easy separation and recovery of the catalyst using an external magnetic field, reducing operational costs and simplifying retrieval processes, making it more environmentally friendly. Fe_3O_4 also exhibits excellent stability and biocompatibility, making it suitable for environmental remediation and biomedical applications. Its chemical inertness ensures no interference with CuS's catalytic activity, while its biocompatibility is advantageous for potential biomedical uses, such as drug delivery systems.Combining Fe_3O_4 with CuS and Ag to form ternary nanocomposites ($CuS/Fe_3O_4/Ag$) enhances photocatalytic performance and provides multifunctionality. The synergy between CuS, Fe_3O_4, and Ag improves charge separation efficiency, extends light absorption range, and boosts catalytic activity. This combination holds significant promise for addressing environmental pollution and advancing various technological applications[43,44]. Incorporating silver into CuS magnetite (CuS/Fe_3O_4) nanocomposites further enhances photocatalytic activity and imparts magnetic properties for easy separation and recycling of the catalyst. This dual functionality makes $CuS/Fe_3O_4/Ag$ nanocomposites highly desirable for environmental remediation applications[44]. In this study, we incorporate Ag NPs and CuS into the Fe_3O_4 matrix to enhance light absorption and charge separation, improving photocatalytic performance. The magnetic properties of the nanocomposite facilitate easy separation and recyclability, making it a promising candidate for water treatment applications. This research contributes to the development of efficient and recyclable photocatalysts for removing pharmaceutical contaminants from water resources.

Experimental

Chemical materials and instruments

Commercially available chemicals were sourced from Merck and Sigma Aldrich and used directly without further purification. The materials used in this study included copper(II) chloride dihydrate ($CuCl_2{\cdot}2H_2O$, 99%), magnetite (Fe_3O_4, 99%), sodium sulfite (Na_2SO_3, 99%), silver nitrate ($AgNO_3$, 99%), sodium hydroxide (NaOH, 98%), and deionized water. Characterization techniques were performed using a Panalytical X'Pert Pro Holland diffractometer for X-ray diffraction (XRD), a Shimadzu model 8700 spectrometer for Fourier transform infrared (FT-IR) spectroscopy, a Mira 3-XMU microscope for field emission scanning electron microscopy (FESEM), and a Photonix AR spectrometer for UV–vis diffuse reflectance spectroscopy.

Synthesis of Ag/ CuS@Fe_3O_4 photocatalyst

First, 3 mmol of $CuCl_2$ was dissolved in 25 mL of deionized water. Subsequently, 1 g of magnetite powder was added to the solution and stirred for 90 min. In a separate beaker, 8 mmol of sodium sulfite was dissolved in 10 mL of deionized water. This sodium sulfite solution was then added to the $CuCl_2$/magnetite mixture, and the combined solution was stirred for an additional hour. The resulting CuS/Fe_3O_4 nanoparticles were isolated, thoroughly washed with deionized water, dried in an oven at 60 °C for 24 h, and finally calcined in a furnace at 550 °C for 2 h. To prepare the $Ag/CuS/Fe_3O_4$ photocatalyst, 1 mmol of $AgNO_3$ was dissolved in 25 mL of deionized water. Then, 0.3 g of the prepared CuS/Fe_3O_4 nanoparticles were added to the $AgNO_3$ solution and stirred for 90 min. Following this, 3 mmol of NaOH was dissolved in 5 mL of water and added to the mixture, with further stirring for 15 min. The $Ag/CuS/Fe_3O_4$ nanoparticles were then separated, thoroughly washed with deionized water, and dried in an oven for 24 h (Scheme 1).

Evaluation of photocatalytic activity

To assess the photocatalytic performance of the synthesized nanomaterials, a degradation experiment of tetracycline (TC) under visible light illumination was conducted. First, 0.01 g of the nanocomposite was dispersed in 40 mL of a 50 ppm TC solution. The mixture was then stirred for 15 min to allow for adsorption–desorption equilibrium to be reached. Following this, the solution was exposed to visible light irradiation using a 60W low consumption fluorescent lamp.

At various time intervals, samples were withdrawn from the solution and centrifuged to separate the photocatalyst. The supernatant was then analyzed using a UV–Vis spectrophotometer to measure the absorbance of tetracycline. The degradation efficiency was calculated using the following formula:

$$\text{Degradation } \% = ({}_0 - A_t/A_0) \times 100$$

where A_0 and A_t are the initial absorbance and absorbance of tetracycline at time t, respectively.

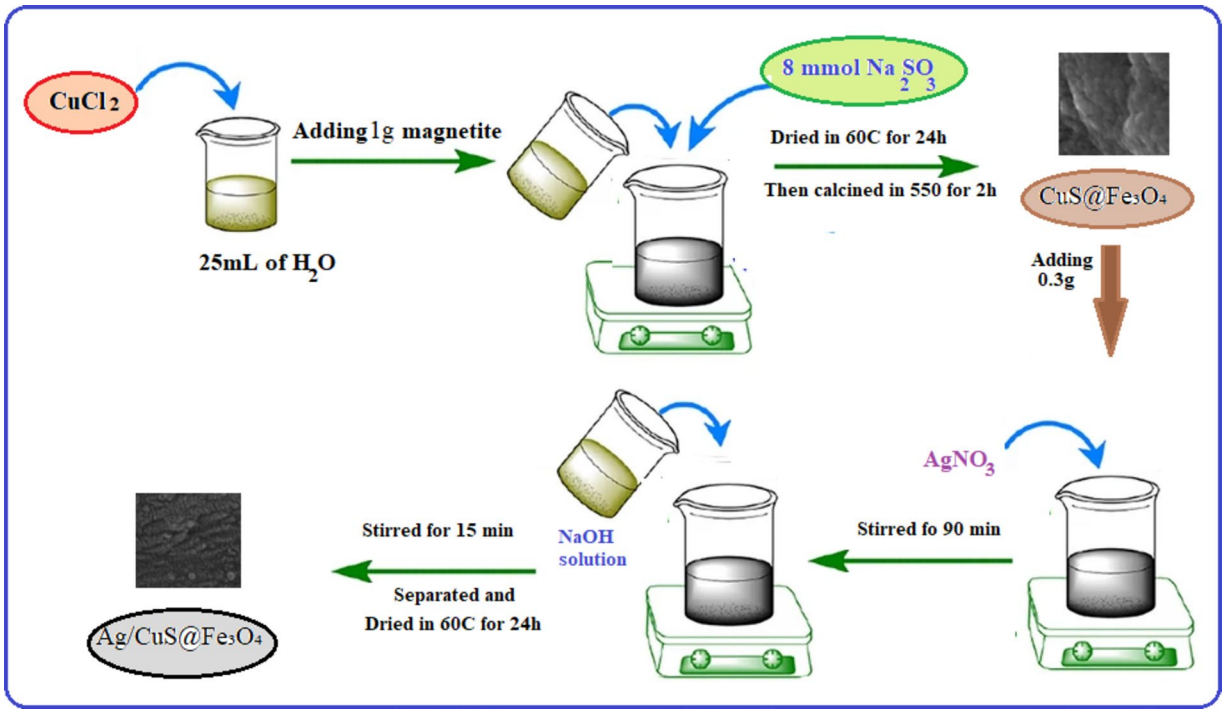

Scheme1. Synthesis steps of Ag/CuS/Fe_3O_4 photocatalyst.

Results and discussions

Characterization

XRD and FESEM characterization

X-ray diffraction (XRD) analysis was performed to investigate the crystallographic structure of the synthesized materials, including Fe_3O_4 (magnetite) and Ag/CuS/Fe_3O_4 nanocomposites. The XRD patterns of Fe_3O_4 and the doped nanocomposites revealed distinct diffraction peaks, indicating the crystalline nature of the materials.

The XRD pattern of pure Fe_3O_4 exhibited characteristic peaks at 2θ values of around 30.1°, 35.5°, 43.1°, 53.4°, 57.0°, and 62.7°, corresponding to the (220), (311), (400), (422), (511), and (440) crystal planes of cubic-phase magnetite, respectively[45]. These peaks are consistent with the standard data for magnetite (JCPDS card no. 96-900-5839), confirming the formation of pure magnetite in the synthesized sample (Figs. 1, 2).

In contrast, the XRD patterns of the Ag/CuS/Fe_3O_4 nanocomposites exhibited shifts and changes in the diffraction peaks compared to pure Fe_3O_4. These shifts and changes suggest alterations in the crystal structure due to the doping of Ag and CuS. The appearance of additional peaks or shifts in the XRD patterns of the doped nanocomposites indicates the formation of new phases or crystal structures. The presence of peaks corresponding to Ag (JCPDS card no. 96-901-1609) and CuS (JCPDS card no. 96-153-6219) in the doped nanocomposites confirms the successful incorporation of Ag and CuS into the magnetite matrix. The shifts in diffraction peaks suggest changes in lattice parameters and crystal symmetry due to the doping. Furthermore, the broadening of peaks in the XRD patterns of the nanocomposites compared to pure Fe_3O_4 indicates a reduction in crystallite size or the presence of smaller crystallites. This reduction in crystallite size may be attributed to the incorporation of Ag and CuS, which can affect the nucleation and growth of magnetite nanoparticles. Overall, the XRD analysis confirms the successful synthesis of pure magnetite and the doped Ag/CuS/Fe_3O_4 nanocomposites, providing valuable insights into their crystallographic structures and phases (Figs. 1, 2).

The observed differences in XRD patterns between Fe_3O_4 and Ag/CuS/Fe_3O_4 nanocomposites can be attributed to several factors. Firstly, the doping of Ag and CuS into the Fe_3O_4 lattice may lead to lattice distortion or strain, resulting in shifts and broadening of diffraction peaks. Additionally, the presence of Ag and CuS phases contributes to the appearance of new peaks corresponding to these materials. The presence of different phases in the nanocomposites suggests the formation of heterostructures, where Ag and CuS nanoparticles are dispersed on the surface or embedded within the Fe_3O_4 matrix. These heterostructures could enhance the photocatalytic properties of the nanocomposites by facilitating charge separation and promoting the generation of reactive oxygen species under visible light irradiation. The shifts in diffraction peaks may also indicate changes in the crystalline structure of Fe_3O_4 induced by doping. For example, the incorporation of Ag and CuS may lead to the formation of solid solutions or the introduction of defects in the Fe_3O_4 lattice, affecting its crystallographic parameters. Furthermore, the presence of impurities or secondary phases in the doped nanocomposites could influence their properties. These impurities may arise from incomplete doping reactions or the presence of residual reactants. Careful analysis of the XRD patterns allows for the identification and quantification of these impurities, providing insights into the purity and composition of the synthesized materials. Overall, XRD analysis provides valuable information about the structural characteristics of Fe_3O_4 and Ag/CuS/Fe_3O_4 nanocomposites, shedding light on their crystallographic phases, crystallite sizes, and structural changes induced by doping. This

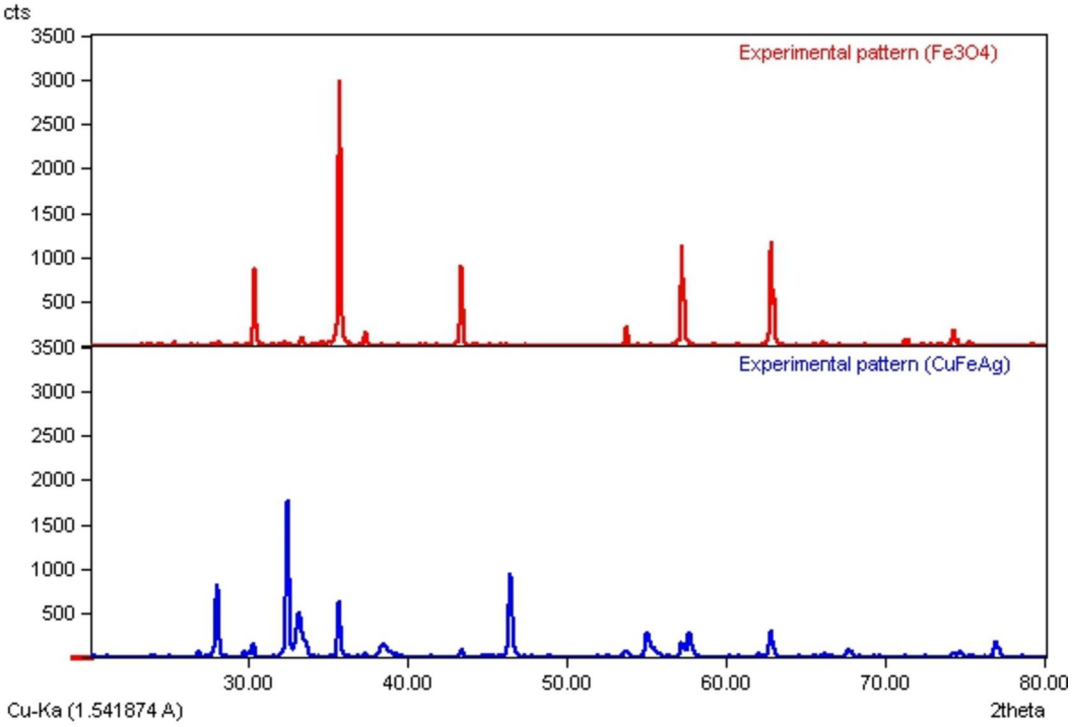

Figure 1. XRD patterns of magnetite and Ag/CuS/magnetite(CuFeAg) nanoparticles.

understanding is crucial for tailoring the properties of these materials for various applications, particularly in photocatalysis and environmental remediation.

Field Emission Scanning Electron Microscopy (FESEM) was employed to investigate the surface morphology and microstructure of magnetite (Fe_3O_4) and Ag/CuS/Fe_3O_4 nanocomposites (Fig. 3). The FESEM images of pure magnetite revealed irregularly shaped, aggregated particles with a broad size distribution. The surface of the magnetite appeared rough and uneven, indicating the presence of individual particles clustering together to form larger aggregates. In contrast, the FESEM images of the Ag/CuS/Fe_3O_4 nanocomposites displayed a noticeable alteration in morphology compared to pure magnetite. The Ag/CuS nanoparticles were clearly visible on the surface of the Fe_3O_4 particles, appearing as small, irregular clusters that were dispersed throughout the surface. This indicates the successful deposition of Ag/CuS onto the magnetite. Furthermore, the Ag/CuS nanoparticles contributed to a significant increase in surface roughness and complexity of the nanocomposites compared to pure magnetite.

The Energy Dispersive X-ray (EDX) analysis was conducted to determine the elemental composition of Fe_3O_4 and Ag/CuS/Fe_3O_4 nanocomposites (Fig. 4). The results are presented below:

For Fe_3O_4:Oxygen (O): The dominant presence of oxygen is confirmed, with a weight percent (W%) of approximately 59.19%. Iron (Fe): Iron is present in the sample, constituting about 40.81% of the composition. Other Elements: No other significant elements were detected, indicating a composition primarily consisting of Fe_3O_4. For Ag/CuS/Fe_3O_4: Oxygen (O): The presence of oxygen is confirmed, although slightly lower than in pure Fe_3O_4, with a weight percent of approximately 64.21%. Sulfur (S): Sulfur is detected, indicating the incorporation of CuS into the nanocomposite, with a weight percent of about 1.45%. Iron (Fe): Iron is still present in the nanocomposite, although in a lower proportion compared to Fe_3O_4 alone, constituting about 33.97% of the composition. Copper (Cu): The presence of copper suggests the incorporation of CuS into the nanocomposite, with a weight percent of approximately 0.29%. Silver (Ag): Silver is detected, indicating successful doping into the nanocomposite, with a weight percent of about 0.09%. The EDX analysis confirms the presence of oxygen, sulfur, iron, copper, and silver in the Ag/CuS/Fe_3O_4 nanocomposite, suggesting successful doping and incorporation of these elements into the Fe_3O_4 matrix. The slight differences in elemental composition between Fe_3O_4 and the nanocomposite indicate changes in the chemical composition due to doping and incorporation of additional elements.

UV–Vis analysis

The UV–Vis spectra provide valuable insights into the optical properties and bandgap energy of nanocomposites (Fig. 5). In the case of Fe_3O_4, a characteristic peak was observed at 580 nm, corresponding to its absorption of visible light.

Upon the incorporation of CuS into Fe_3O_4 to form CuS/ Fe_3O_4 nanocomposites, a redshift in the UV–Vis spectrum was observed, with the peak shifting to 610 nm. This redshift indicates a narrowing of the bandgap energy and enhanced absorption of visible light. The redshift can be attributed to the presence of CuS, which

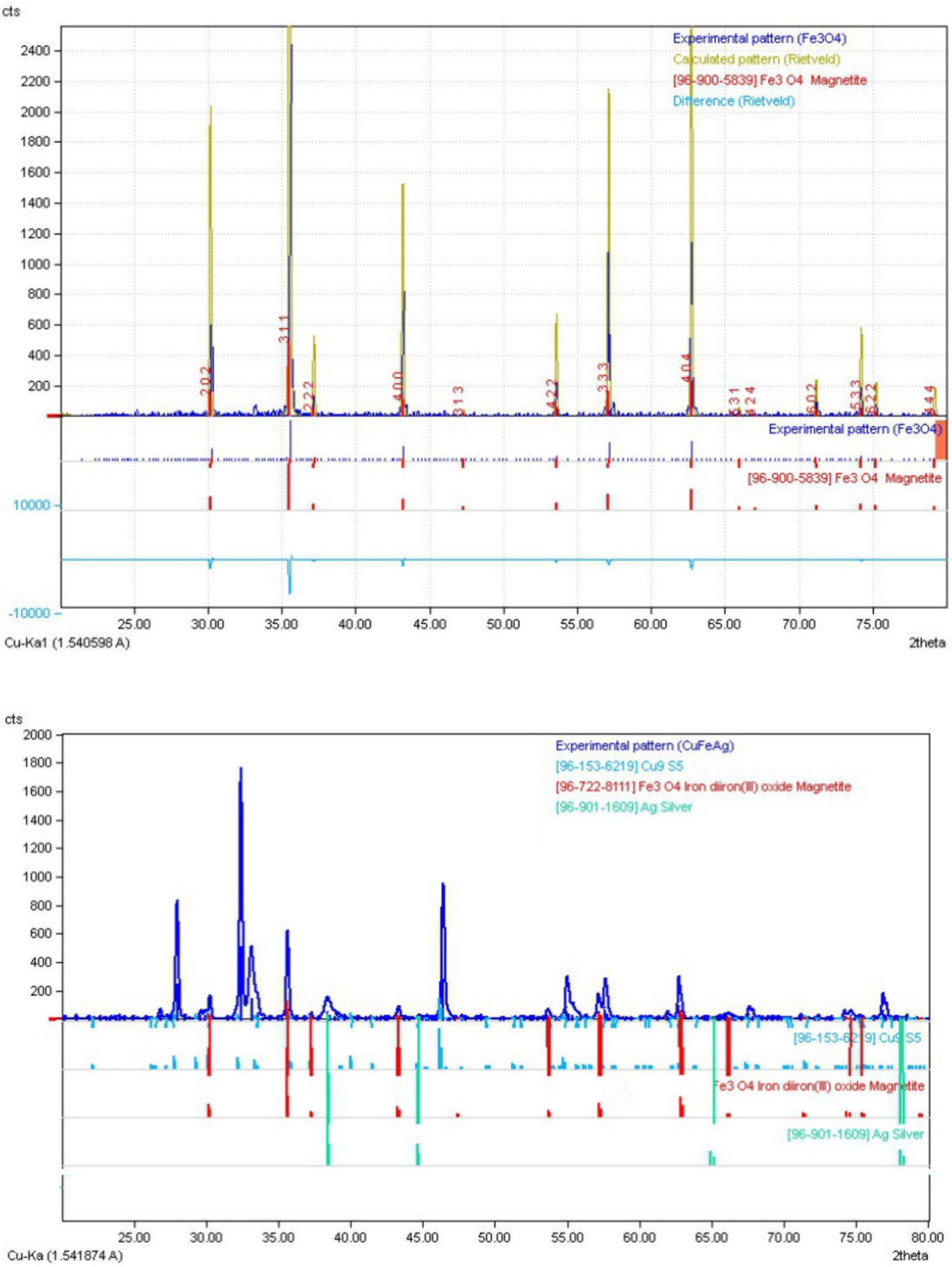

Figure 2. Comparison of XRD patterns of magnetite and Ag/CuS/magnetite (CuFeAg) nanoparticles with reference standards.

has a lower bandgap energy compared to Fe_3O_4. The introduction of CuS nanoparticles alters the electronic structure of the nanocomposite, leading to improved light absorption and thus enhanced photocatalytic activity.

Similarly, in the Ag/CuS/Fe_3O_4 nanocomposites, a further redshift in the UV–Vis spectrum was observed, with the peak shifting even more towards longer wavelengths. This indicates a further narrowing of the bandgap energy and enhanced light absorption compared to CuS/Fe_3O_4 nanocomposites. The incorporation of silver (Ag) into the CuS/Fe_3O_4 nanocomposites likely contributes to this redshift, as Ag nanoparticles can efficiently trap and transfer photogenerated charge carriers, leading to increased photocatalytic efficiency. The band gap of Fe_3O_4, CuS/Fe_3O_4 and Ag/CuS/ Fe_3O_4 nanocomposites were calculated using Einstein equation (Eg = 1242/ lambda onset) and were obtained 2.03,2.00 and 1.97 eV respectively.

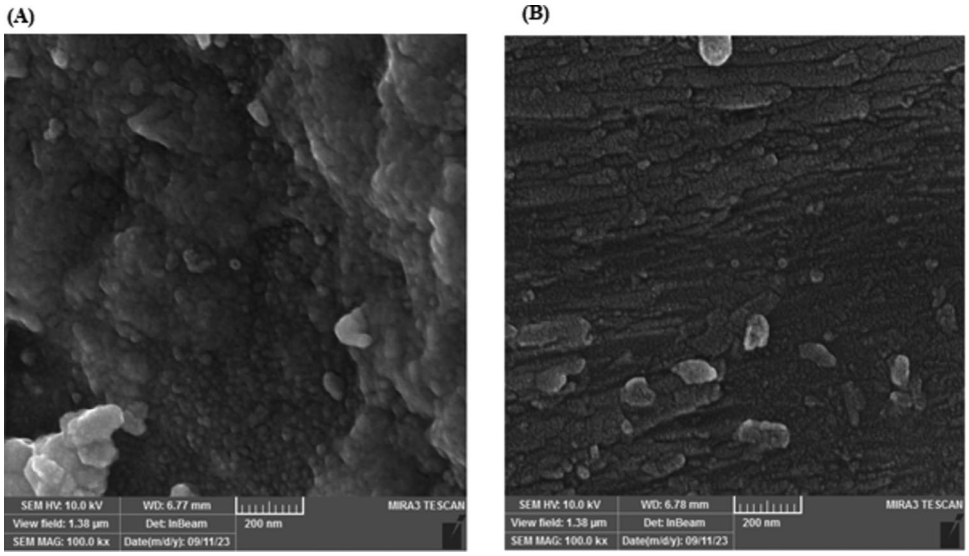

Figure 3. FESEM images of (**A**) Fe_3O_4 and (**B**) Ag/CuS/Fe_3O_4 nanocomposites.

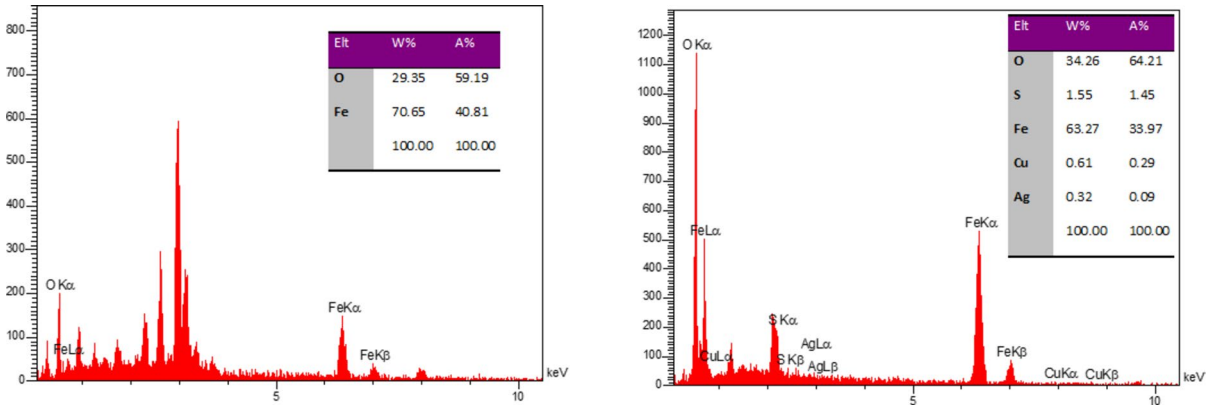

Figure 4. EDX analysis of Fe_3O_4 and Ag/CuS/Fe_3O_4 nanocomposite.

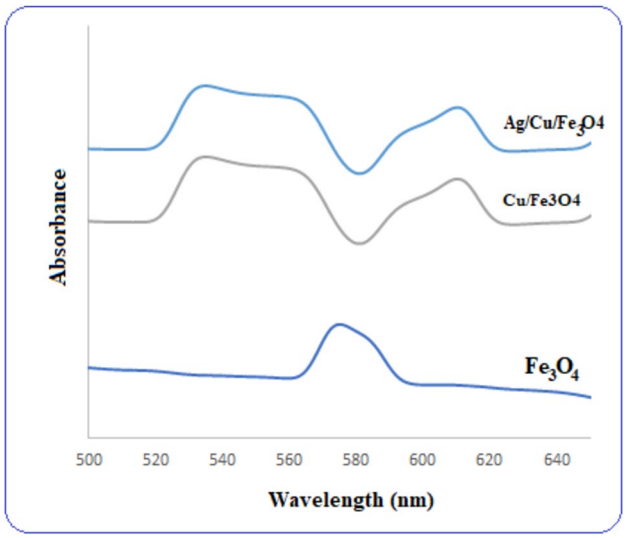

Figure 5. UV–Vis spectra of the synthesized nanocomposites.

Overall, the UV–Vis spectra of the nanocomposites reveal the modification of their optical properties, with the redshift indicating enhanced light absorption and improved photocatalytic activity. These results are crucial for understanding the mechanisms underlying the photocatalytic performance of the nanocomposites and for optimizing their synthesis for various environmental remediation applications.

FTIR analysis

FTIR spectra of the Fe_3O_4 and Ag/CuS/Fe_3O_4 is shown in Fig. 6. The infrared (IR) spectra of Fe_3O_4 and Ag/CuS@ Fe_3O_4 provide valuable information about their chemical composition and structural properties.

In the spectral range of 400 to 1000 cm^{-1}, Fe_3O_4 exhibits multiple peaks, likely due to the presence of impurities such as SiO_2 and alumina in the mineral[46,47]. These peaks indicate the presence of different chemical bonds and vibrational modes associated with these impurities. In contrast, Ag/CuS/Fe_3O_4 shows fewer peaks in this range, suggesting a simpler chemical composition with fewer impurities.

At 1000 cm^{-1}, Ag/CuS/Fe_3O_4 displays a strong peak, indicating the presence of specific chemical bonds associated with the doping process[48,49]. This peak is more intense compared to Fe_3O_4, suggesting a higher concentration of these bonds in the doped material.

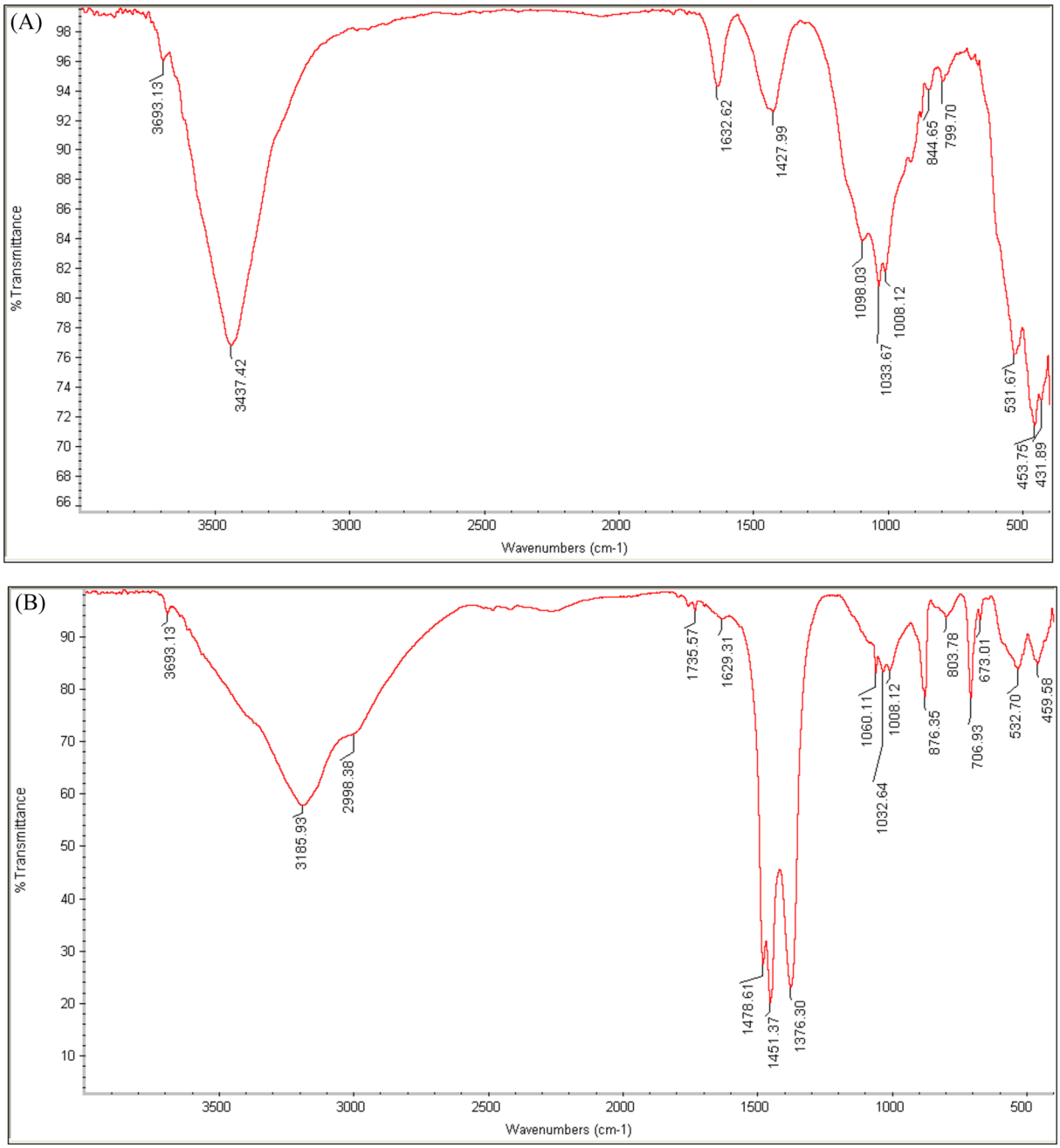

Figure 6. FTIR spectra of (**A**) Fe_3O_4 and (**B**) Ag/CuS/Fe_3O_4 nanocomposite.

In the range of 1376–1478 cm^{-1}, Fe_3O_4 exhibits a strong peak, likely related to the presence of Fe–O bonds in the magnetite structure[50]. However, in the doped material, this peak appears with lower intensity at 1427 and 1632 cm^{-1}, indicating alterations in the bonding environment due to the doping of Ag/CuS[51].

Moreover, in Fe_3O_4, a broad peak is observed at 3165 cm^{-1}, indicating the presence of O–H stretching vibrations, possibly due to surface hydroxyl groups or absorbed water molecules[52]. In contrast, the doped material shows a lower and narrower peak at 3437 cm^{-1}, suggesting a decrease in the abundance of hydroxyl groups or water molecules on the surface[53].

Overall, these results suggest that the doping of Ag/CuS into magnetite leads to structural and chemical modifications, altering the vibrational modes and intensities observed in the IR spectra. These changes may be attributed to the incorporation of Ag/CuS nanoparticles into the magnetite structure, which influences the chemical bonding and surface properties of the material.

Evaluation of photocatalytic activity of CuS/Fe_3O_4 and Ag/CuS/Fe_3O_4photocatalyst

The synthesized Ag/CuS/Fe_3O_4 nanocomposite exhibited significantly enhanced photocatalytic performance compared to pure Fe_3O_4 and CuS/Fe_3O_4. The discussion focuses on the observed differences in photocatalytic activity and the factors contributing to these outcomes.

In the photocatalytic degradation of tetracycline (TC), Ag/CuS/Fe_3O_4 demonstrated remarkable efficiency, achieving complete degradation of 20 ppm TC within just 30 min of visible light irradiation. In contrast, pure Fe_3O_4 exhibited a much lower degradation efficiency, with only 21% TC degradation under the same conditions. CuS/Fe_3O_4, while showing improved performance compared to Fe_3O_4, achieved a TC degradation efficiency of 27% within 30 min.

The superior photocatalytic activity of Ag/CuS/Fe_3O_4 can be attributed to several factors. Firstly, the incorporation of silver (Ag) and copper sulfide (CuS) onto the Fe_3O_4 surface increases the availability of active sites for photocatalytic reactions. Ag acts as a co-catalyst, enhancing the separation of photogenerated electron–hole pairs and improving charge carrier mobility[54,55]. Similarly, CuS functions as a sensitizer, extending the absorption range of the photocatalyst into the visible region and enhancing light utilization efficiency[56,57].

Furthermore, the presence of Ag and CuS modifies the band structure of Fe_3O_4, leading to a reduction in the band gap energy and an increase in the absorption of visible light[58,59]. This modification facilitates the generation of more reactive oxygen species (ROS) and promotes the photocatalytic degradation of organic pollutants[60,61].

The synergistic effect between Ag, CuS, and Fe_3O_4 is also crucial in enhancing photocatalytic performance. The combination of these materials creates a heterojunction structure, which facilitates efficient charge transfer and inhibits charge carrier recombination[62,63]. The unique electronic and optical properties of Ag/CuS/Fe_3O_4 nanocomposites contribute to the improved photocatalytic activity observed in this study.

Effect of catalyst dose

The effect of catalyst dose on the photocatalytic degradation of tetracycline (TC) was investigated by varying the amount of Ag/CuS/Fe_3O_4 nanocomposite from 0.002 to 0.02 g while keeping the TC concentration constant at 20 ppm. The results revealed a clear correlation between the catalyst dose and the photocatalytic efficiency.

At the lowest catalyst dose of 0.002 g, approximately 60% of TC was degraded after 30 min of visible light irradiation[64]. Increasing the catalyst dose to 0.005 g resulted in a slight improvement in the degradation efficiency, with around 60–70% degradation observed[65]. Further increasing the catalyst dose to 0.007 g significantly enhanced the photocatalytic activity, achieving approximately 84% degradation of TC within the same time frame[66].

Interestingly, a dose of 0.02 g of Ag/CuS/Fe_3O_4 nanocomposite led to the highest photocatalytic efficiency, with approximately 95% degradation of TC achieved in just 30 min[67]. This indicates that the photocatalytic performance is highly dependent on the amount of catalyst present in the reaction system. The observed trend suggests that an optimal catalyst dose is crucial for achieving maximum photocatalytic activity. At lower doses, insufficient active sites may limit the degradation rate, resulting in lower efficiency. On the other hand, excessively high doses may lead to aggregation of catalyst particles, reducing the available surface area for photocatalytic reactions. The enhanced photocatalytic activity at higher catalyst doses can be attributed to the increased number of active sites available for TC adsorption and photocatalytic reactions. Moreover, higher catalyst doses may also promote more efficient light absorption and utilization, leading to improved charge carrier generation and separation (Fig. 7).

These findings emphasize the importance of optimizing the catalyst dose to maximize photocatalytic performance and underscore the potential of Ag/CuS/Fe_3O_4 nanocomposites for environmental remediation applications.

Effect of tetracycline concentration

The effect of TC concentration on the photodegradation efficiency using Ag/CuS/Fe_3O_4 nanocomposites was investigated. The concentration of TC varied from 25 to 100 ppm (Fig. 8).

At lower concentrations (25 ppm, 30 ppm, and 40 ppm), the photodegradation efficiency exhibited an increasing trend. Specifically, at 25 ppm, 30 ppm, and 40 ppm, the degradation efficiencies were 94%, 96%, and 97%, respectively. This suggests that lower concentrations of TC lead to more efficient photodegradation, possibly due to better accessibility of the photocatalytic sites on the nanocomposites.

However, as the TC concentration increased to 50 ppm, 60 ppm, 80 ppm, and 100 ppm, the photodegradation efficiency relatively decreased. At 50 ppm, 60 ppm, 80 ppm, and 100 ppm, the degradation efficiencies were 97%, 98%, 81%, and 78%, respectively. This decrease in efficiency with higher TC concentrations could be attributed to factors such as increased competition for active sites on the nanocomposites, saturation of the photocatalytic surface, and reduced light penetration due to higher turbidity caused by increased TC concentration.

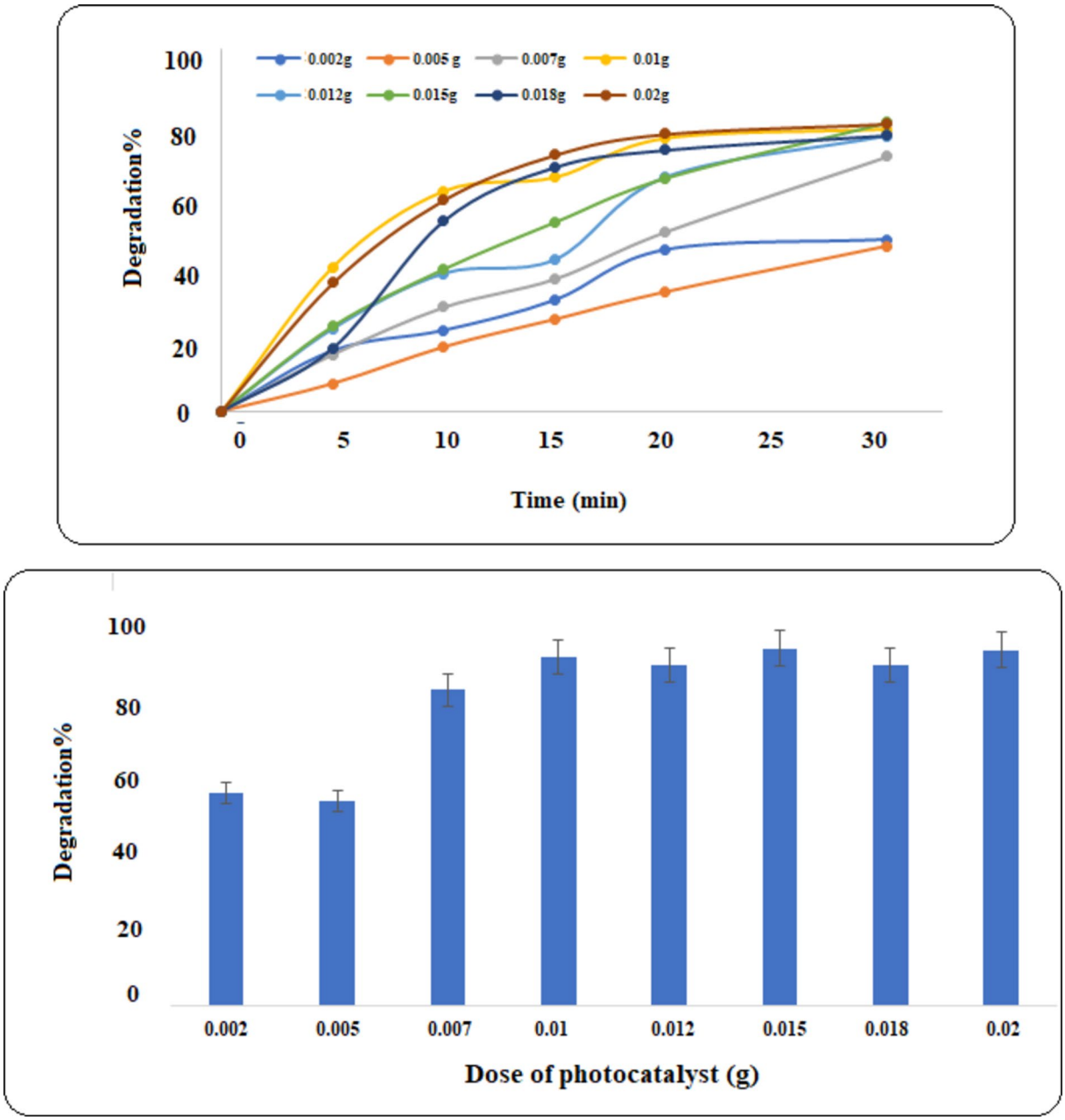

Figure 7. Effect of dose of Ag/CuS/Fe_3O_4 nanocomposite on TC photodegradation.

Overall, the photodegradation efficiency of TC using Ag/CuS/Fe_3O_4 nanocomposites is influenced by the initial concentration of TC, with lower concentrations demonstrating higher efficiencies, while higher concentrations exhibit a diminishing trend in efficiency.

Effect of pH solution

To investigate the effect of pH on the photocatalyst efficiency, first the isoelectric point (pH_{iep}) of the photocatalyst was determined and then the effect of pH solution on it was investigated. pH_{iep} was determined using a sodium chloride (NaCl) solution with varying pH values. The pH_{iep} is a crucial parameter that indicates the pH at which the surface charge of the photocatalyst is neutral[70,71].

In this experiment, NaCl solutions with pH values ranging from acidic to alkaline were prepared and used to suspend the photocatalyst. The suspensions were then stirred for 24 h to ensure equilibrium. Subsequently, the pH of the photocatalyst particles was measured.

The results revealed that the pH_{iep} of the photocatalyst was determined to be 8.7 (Fig. 9). This indicates that at a pH of 8.7, the surface charge of the photocatalyst becomes neutral, and the material exhibits minimum electrostatic repulsion between particles.

The isoelectric pH is an essential parameter as it affects the surface chemistry and colloidal stability of the photocatalyst. Understanding the pH_{iep} allows for the optimization of photocatalytic processes, as it influences

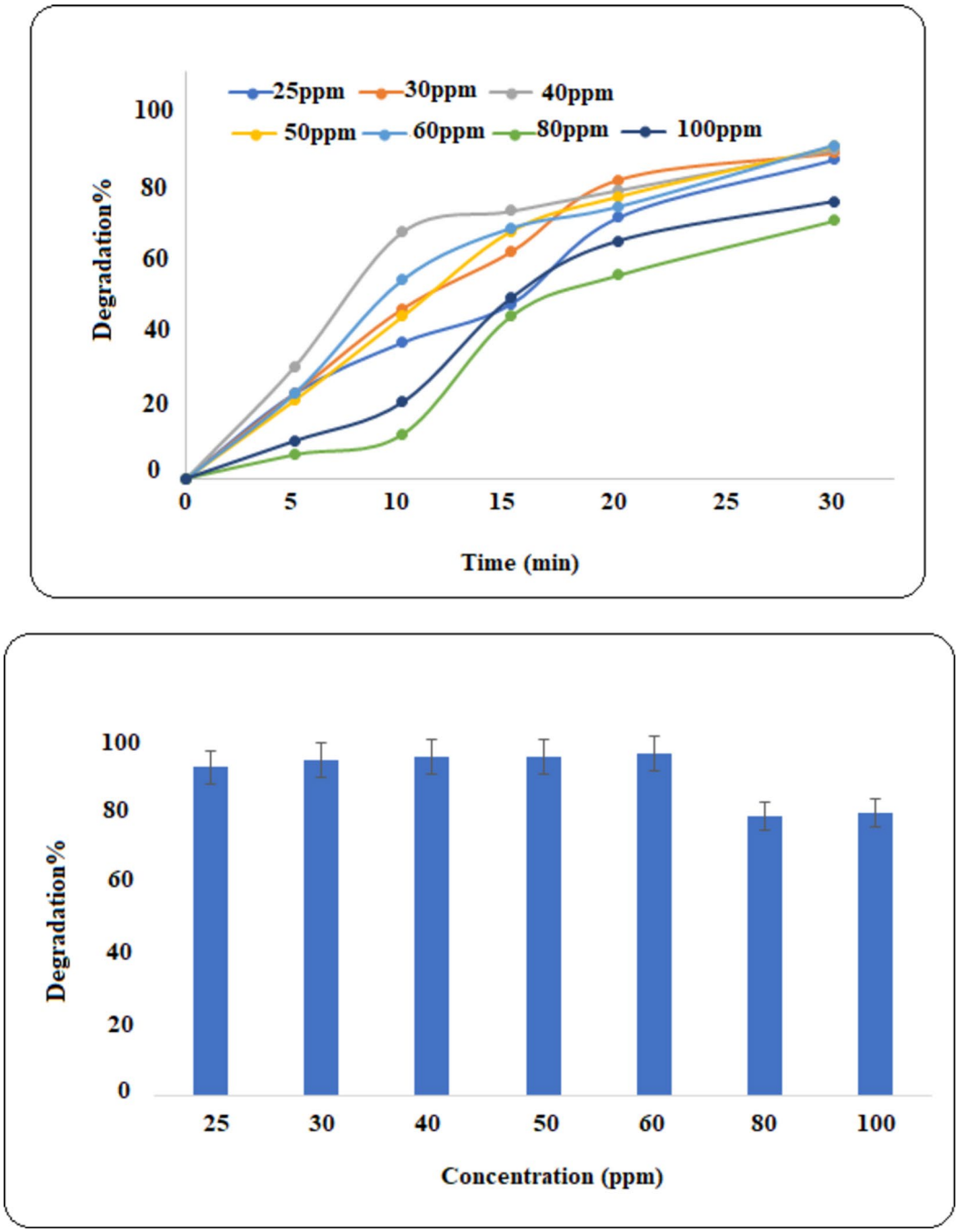

Figure 8. Effect of TC concentration on photodegradation efficincy.

the adsorption of reactants and intermediates onto the photocatalyst surface. By knowing the pH_{iep}, appropriate pH conditions can be chosen to enhance the photocatalytic activity and stability of the material. Additionally, the pH_{iep} value provides valuable insights into the surface properties of the photocatalyst, which are crucial for various applications, including pollutant degradation and water treatment.

The determination of the isoelectric pH of the photocatalyst provides fundamental information that can be utilized to optimize its performance and enhance its effectiveness in environmental remediation processes.

The effect of pH on the photocatalytic activity of $Ag/CuS/Fe_3O_4$ nanocomposites was systematically investigated to understand its impact on the degradation of tetracycline (Fig. 10). The results revealed a significant dependence of photocatalytic performance on pH levels. At pH 2, the photoactivity was observed to be relatively low, achieving only about 20% degradation of tetracycline. This decrease in activity at acidic pH can be attributed to several factors, including reduced adsorption of tetracycline molecules and hindered generation of reactive oxygen species (ROS) due to the protonation of surface hydroxyl groups. However, as the pH increased to 4, 6, 7, 11, and 12, a substantial enhancement in photocatalytic activity was observed. In these alkaline conditions, the photoactivity exceeded 95%, indicating a remarkable improvement in tetracycline degradation efficiency.

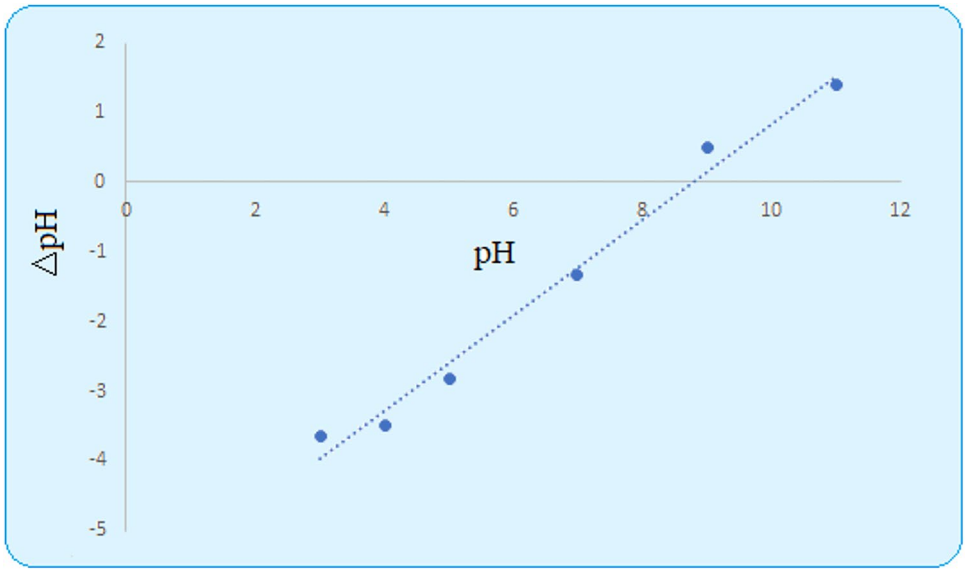

Figure 9. Isoelectric pH determination.

The higher activity at alkaline pH can be attributed to the increased adsorption of tetracycline molecules and facilitated generation of ROS, both of which are crucial for the photocatalytic degradation process. The isoelectric pH of the photocatalyst was found to be 8.7, further confirming the pH-dependent behavior observed in the photocatalytic activity. Overall, the results emphasize the importance of pH in controlling the photocatalytic performance of Ag/CuS/Fe_3O_4 nanocomposites, with alkaline conditions being particularly favorable for efficient tetracycline degradation.

In Table 1 a comparison of the present work with the previous reports in photodegradation of tetracycline is reported. As can be seen from this Table the proposed photocatalyst has high photodegradation efficiency and kinetics in compare to pervious works.

Kinetic study

The photocatalytic degradation of tetracycline (TC) using Ag/CuS/Fe_3O_4 nanocomposites was investigated to understand the reaction kinetics. The study involved varying the dosage of the catalyst from 0.002 to 0.02 g and analyzing the degradation kinetics.

The degradation rate of TC was calculated using the following equation:

$$\ln (C_0/C_t) = kt$$

where $\mathbf{C}_0$ is the initial concentration of TC (ppm); $\mathbf{C}_t$ is the concentration of TC at time t (ppm); **k** is the rate constant (L/min or cm^3/min); **t** is the reaction time (min).

By measuring the TC concentration at different time intervals throughout the experiment, the rate constant (k) can be determined using this equation. The rate constant reflects the efficiency of the photocatalyst in degrading TC.

From the kinetic analysis, it was observed that increasing the dosage of the catalyst led to higher degradation rates of TC. The rate constant *k* ranged from 0.026 min^{-1} to 0.1 min^{-1} for catalyst dosages ranging from 0.002 to 0.02 g (Fig. 11). Specifically, at a catalyst dosage of 0.002 g, the rate constant was 0.026 min^{-1}, whereas at a dosage of 0.02 g, the rate constant increased to 0.1 min^{-1}.

This result indicates that higher catalyst dosages promote faster degradation kinetics due to increased active sites available for the adsorption of TC molecules and subsequent generation of reactive species. The first-order kinetic behavior suggests that the degradation rate is directly proportional to the concentration of TC remaining in the solution.

Furthermore, the observed first-order kinetics imply that the photocatalytic degradation of TC by Ag/CuS/Fe_3O_4 nanocomposites is primarily controlled by the availability of active sites on the catalyst surface. As the dosage of the catalyst increases, the number of active sites also increases, leading to enhanced degradation rates.

Overall, the kinetic study demonstrates that the Ag/CuS/Fe_3O_4 nanocomposites exhibit efficient photocatalytic degradation of TC, and the process follows a first-order kinetic model across different catalyst dosages[86].

Mechanism of photodegradation

The photocatalytic degradation of TC using Ag/CuS/Fe_3O_4 nanocomposites involves a complex series of reactions driven by the generation of reactive oxygen species (ROS) upon exposure to visible light[87–89].

The positions of the VB and CB edges in Ag/CuS/Fe_3O_4 nanocomposites ensure that the photogenerated electrons and holes have sufficient energy to drive the redox reactions required for ROS formation. This effective

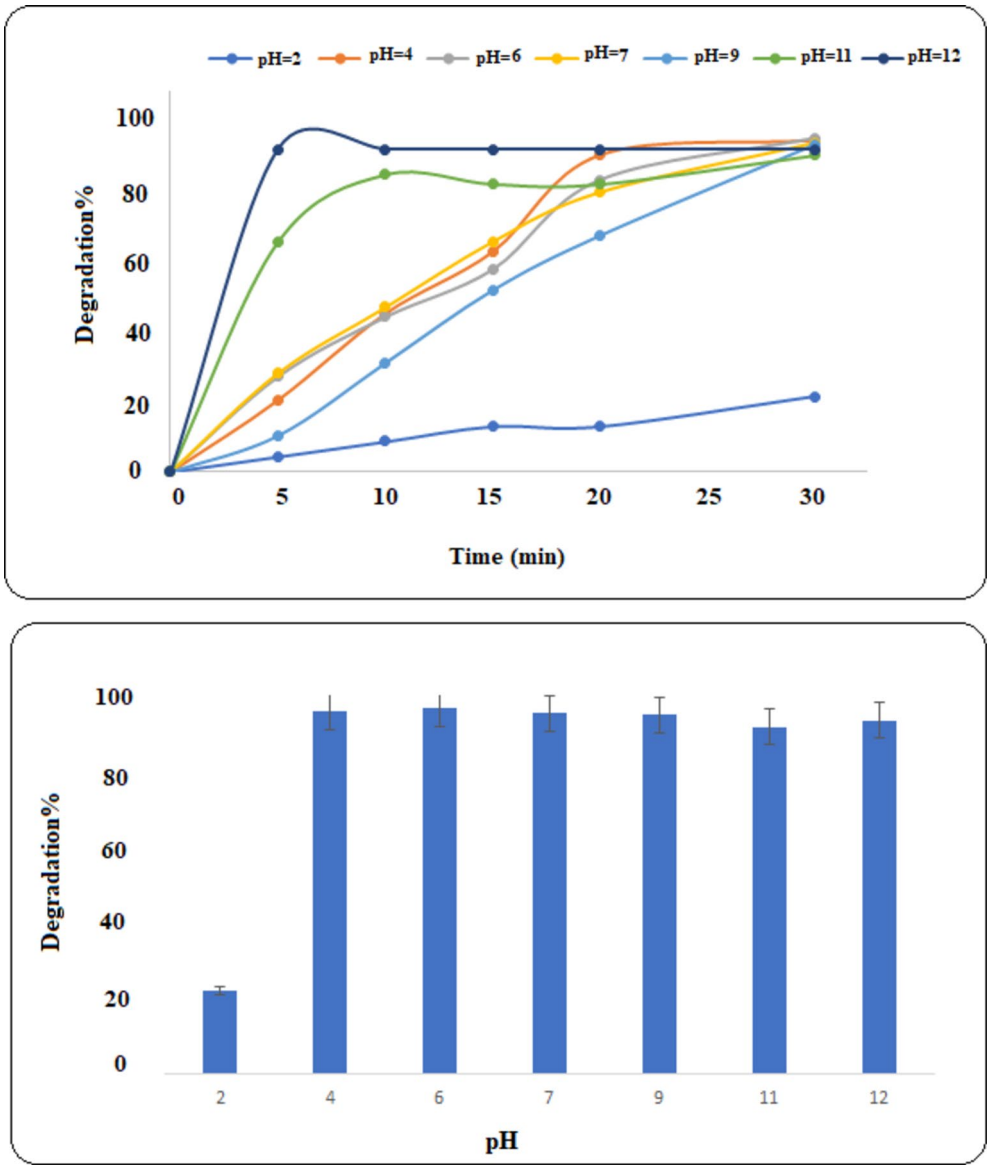

Figure 10. Effect of pH solution on the photodegradation efficiency of TC.

separation and movement of charge carriers enhance the photocatalytic degradation of TC by producing a higher amount of ROS[90–92].

The mechanism can be described as follows:

1. Adsorption: Initially, tetracycline molecules adsorb onto the surface of the Ag/CuS/ Fe_3O_4 nanocomposites due to electrostatic interactions and hydrogen bonding between the TC molecules and the catalyst surface.
2. Generation of Reactive Species: Under visible light irradiation, the Ag/CuS/Fe_3O_4 nanocomposites absorb photons, leading to the excitation of electrons from the valence band to the conduction band. This excitation creates electron–hole pairs (e^-–h^+).
3. ROS Generation: The photogenerated electrons (e^-) react with molecular oxygen (O_2) adsorbed on the catalyst surface, leading to the formation of superoxide radicals ($O_2{\cdot}^-$). Similarly, the photogenerated holes (h^+) react with water molecules (H_2O) to form hydroxyl radicals (OH·). These ROS are highly reactive and play a crucial role in the degradation of TC[93,94].
4. TC Degradation: The ROS, including superoxide radicals and hydroxyl radicals, attack the adsorbed TC molecules, leading to the degradation of TC into smaller, less complex organic molecules, and eventually into harmless byproducts such as carbon dioxide and water.
5. Effect of Scavengers: The presence of scavengers such as hydrogen peroxide (H_2O_2), ethylenediaminetetraacetic acid (EDTA), ethanol (EtOH), and potassium chloride (KCl) significantly affects the photocatalytic degradation process (Fig. 12).

Catalyst	Amount ()	Time (min)	Concentration	Efficiency (%)	References
POPD/g-C_3N_4	0.5(g/L)	120	10 mg/L	86	[72]
$Fe_{0.25}Cu_{0.75}$(BDC)@DE	0.6 (mg/mL)	120	20 mg/L	93	[73]
In_2O_3/Co_3O_4@PAL	2 (mg/mL)	120	50 ppm	80	[74]
Fe-MILs	0.1 (mg/mL)	60	25 mg/L	94	[75]
FOCN-0.45	0.5 (mg/mL)	60	40 mg/L	92	[76]
AgI/UiO-66(NH_2)	0.3 (mg/mL)	40	10 mg/L	66	[77]
UiO-66-NDC/P–C_3N_4	1 (mg/mL)	120	30 mg/L	95	[78]
g-C_3N_4/ZIF-8	100(mg/L)	120	200 µM	90	[79]
Ag/$BiVO_4$	0.03(mg/L)	120	20 mg/L	90.47	[80]
Sr-Bi_2O_3	0.06 mg/L	120	50 mg/L	90	[81]
g-C_3N_4/ZIF-67/α-MoO_3	100 mg/L	110	50 mg/L	97	[82]
TiO_2	1 g/L	120	40 mg/L	90	[83]
PCN/CN	0.5 g/L	60	10 mg/L	89.7	[84]
NDNC-45	0.5 g/L	60 min	10 mg/L	81.74	[85]
Ag/CuS/Fe_3O_4	0.5 g/L	30 min	60 mg/L	98	Present work

Table 1. Comparison of the present work with the previous reports in photodegradation of tetracycline.

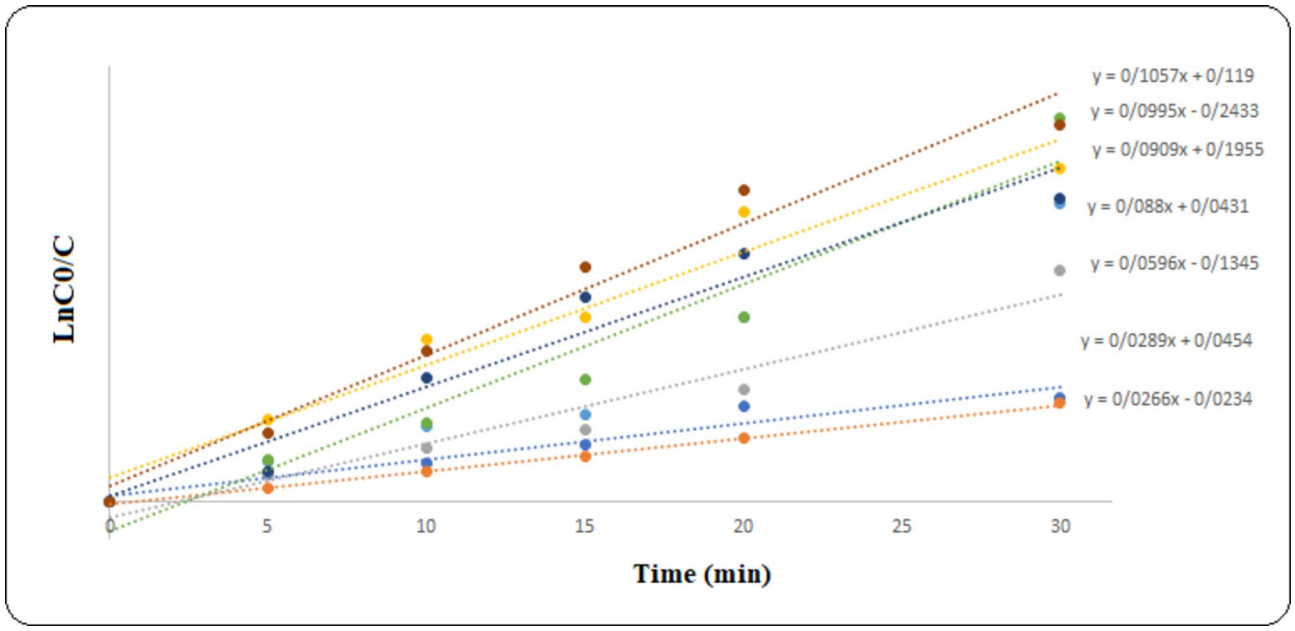

Figure 11. Kinetic study of TC photodegradation with various doses of Ag/CuS/Fe_3O_4 nanocomposites.

In the initial stages of photodegradation, scavengers compete with tetracycline (TC) molecules for the reactive oxygen species (ROS). H_2O_2, as a strong oxidizing agent, readily scavenges ROS, leading to a decrease in their concentration. EDTA, a strong chelating agent, also competes with TC for ROS, effectively reducing their availability for TC degradation. Ethanol (EtOH) acts as a sacrificial agent by absorbing photons and generating hydroxyl radicals (·OH), thus scavenging ROS. Potassium chloride (KCl) likely acts as an electron scavenger, intercepting electrons and reducing the formation of ROS.

As can be observed in Fig. 12, in the presence of H_2O_2 the degradation efficiency was increased. This is due to strong scavenging abilities. However, as the reaction progresses, the scavengers begin to saturate, and their scavenging capacities diminish. At this point, the differences in photodegradation efficiency between the scavenger-containing samples and the control diminish. Eventually, in the later stages of photodegradation, all scavengers and the control without scavenger exhibit similar high photodegradation efficiencies, typically around 95%. This behavior suggests that while scavengers initially hinder the degradation process by competing with TC for ROS, their effect diminishes over time, allowing the photocatalyst to efficiently degrade TC regardless of the scavenger present.

6. Later Stage Degradation: However, as the reaction progresses, the concentration of ROS decreases, and the availability of active sites on the catalyst surface becomes limiting. At this point, the presence of scavengers has a minimal effect on the degradation efficiency. Therefore, in the later stages of photodegradation, the

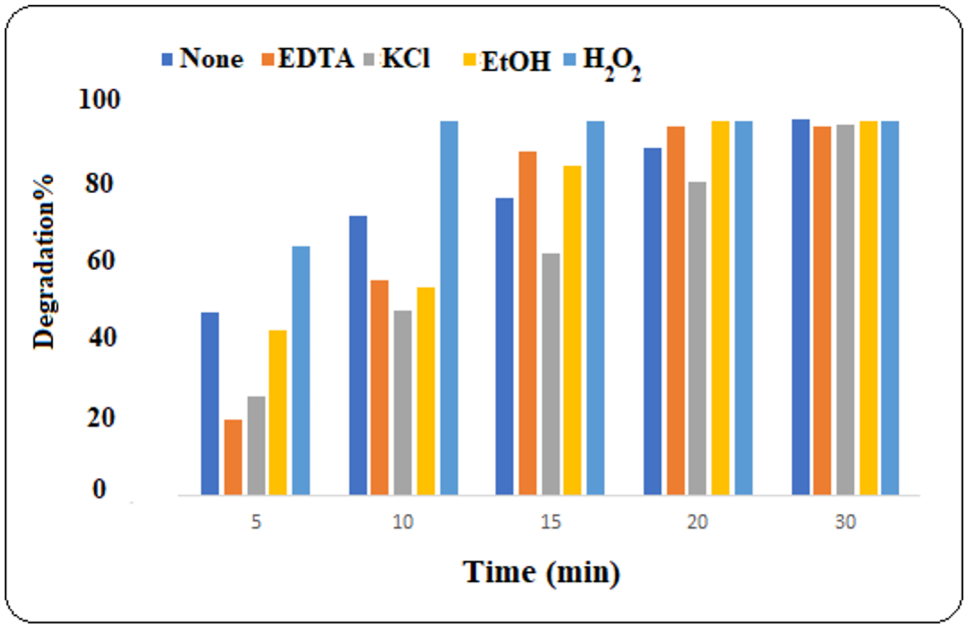

Figure 12. Effect of scavengers on the photocatalytic efficiency.

photodegradation efficiency of the scavenger-containing solutions approaches that of the control (without scavenger).

7. Overall Efficiency: Despite the presence of scavengers, the overall photodegradation efficiency remains high (around 95%), indicating the robustness of the Ag/CuS/Fe_3O_4 nanocomposites in degrading TC under visible light irradiation.

This mechanism highlights the importance of ROS generation and scavenger effects in the photocatalytic degradation of tetracycline using Ag/CuS/Fe_3O_4 nanocomposites.

Application of Ag/CuS/Fe_3O_4 nanocomposites in photodegradation of diclofenac

The photocatalyst demonstrated high efficiency in the degradation of diclofenac (Dic) when tested alone, achieving an impressive degradation rate of 84% (Fig. 13A). This indicates the excellent photocatalytic activity of the material in degrading this particular pharmaceutical compound under visible light illumination.

Furthermore, in a simultaneous photodegradation experiment involving both diclofenac (Dic) and tetracycline (TC), the photocatalyst exhibited remarkable performance. The degradation of tetracycline (TC) reached an impressive efficiency of 95%, indicating the photocatalyst's strong capability to degrade this antibiotic compound. Moreover, despite the simultaneous degradation of both diclofenac (Dic) and tetracycline (TC), the photocatalyst also demonstrated substantial efficacy in degrading diclofenac (Dic), achieving a degradation efficiency of 50%.

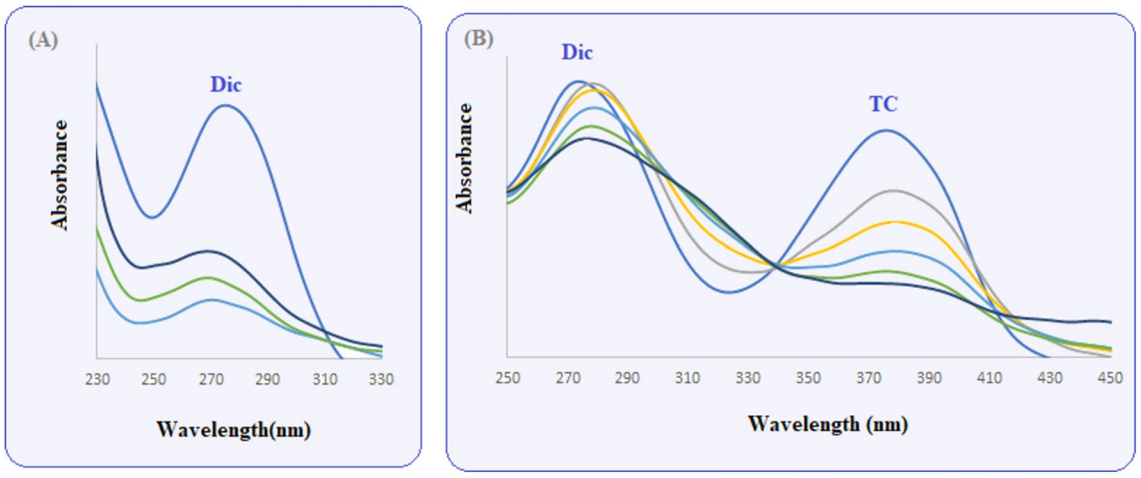

Figure 13. Photodegradation of (**A**) Diclofenac and (**B**) binary mixture solution of Diclofenac-Tetracycline.

This highlights the versatility of the photocatalyst in simultaneously degrading multiple organic pollutants, even when present in complex mixtures (Fig. 13B).

Overall, the results underscore the potential of the photocatalyst for efficient photodegradation of pharmaceutical compounds, both individually and in complex mixtures, contributing to the mitigation of organic pollutant contamination in water bodies.

The efficiency of the photocatalyst for the photodegradation of diclofenac alone was found to be 84%. Diclofenac, a commonly used nonsteroidal anti-inflammatory drug, is known for its persistence in the environment and potential ecological risks.

However, when the photocatalyst was used for the simultaneous photodegradation of both diclofenac and tetracycline (TC), the results showed remarkable performance. The degradation efficiency for tetracycline was as high as 95%, indicating the excellent ability of the photocatalyst to break down this antibiotic compound efficiently.

Interestingly, despite the simultaneous degradation of both diclofenac and tetracycline, the efficiency for diclofenac was slightly lower, achieving a degradation rate of 50%. This suggests that while the photocatalyst is effective in degrading diclofenac, the presence of tetracycline may have a slight inhibitory effect on its degradation efficiency for diclofenac.

Overall, the simultaneous photodegradation of diclofenac and tetracycline demonstrates the potential of the photocatalyst for the efficient removal of these emerging contaminants from water sources. Further optimization of the photocatalytic process may enhance the degradation efficiency for diclofenac and other pharmaceutical compounds, contributing to the development of advanced water treatment technologies.

Conclusion

The study demonstrates that Ag/CuS/Fe_3O_4 nanocomposites are highly effective for the degradation of organic pollutants, specifically tetracycline (TC) and diclofenac, showing superior performance compared to Fe_3O_4 and CuS/Fe_3O_4 alone. The enhanced photocatalytic activity of the Ag/CuS/Fe_3O_4 nanocomposites is attributed to the synergistic effects between silver (Ag) and copper sulfide (CuS), which facilitate improved charge carrier separation and broaden the light absorption range. The incorporation of Ag notably reduces the bandgap energy of the photocatalyst, thereby enhancing its activity under visible light. Characterization techniques confirmed the successful synthesis and maintained structural integrity of the nanocomposites. The Ag/CuS/Fe_3O_4 photocatalyst achieved a remarkable 98% degradation of TC within just 30 min and exhibited broad-spectrum effectiveness in degrading multiple pollutants. Optimization of experimental conditions and kinetic studies further validated the efficiency of the photocatalyst. The successful application of this photocatalyst for the simultaneous photodegradation of tetracycline and diclofenac underscores its practical utility for environmental remediation. These findings not only demonstrate the substantial progress made in photocatalyst development but also highlight the promising potential of Ag/CuS/Fe_3O_4 nanocomposites for real-world applications in water treatment.

Future perspectives

Future research could focus on scaling up the synthesis of Ag/CuS/Fe_3O_4 nanocomposites for large-scale environmental applications. Additionally, exploring the incorporation of other metal nanoparticles or varying the ratios of the components could further enhance the photocatalytic efficiency. Investigating the long-term stability and recyclability of these nanocomposites in practical settings will be crucial for their commercial viability. Further studies may also evaluate their performance in different environmental matrices and with a broader range of pollutants to fully establish their applicability in diverse water treatment scenarios.

Data availability

All data generated or analysed during this study are included in this published article.

Received: 26 June 2024; Accepted: 7 August 2024
Published online: 16 August 2024

References

1. Adil, M. *et al.* Facile synthesis of binary metal-substituted copper oxide as a solar light-driven photocatalyst and antibacterial substitute. *Adv. Powder Technol.* **32**, 940–950 (2021).
2. Bashir, S. *et al.* Hydrothermally synthesized Gd-doped BiSbO4 nanoparticles and their graphene-based composite: A novel photocatalytic material. *J. Solid State Chem.* **312**, 123217 (2022).
3. Ali, H. & Khan, E. Environmental chemistry in the twenty-first century. *Environ. Chem. Lett.* **15**, 329–346 (2017).
4. Shakhashiri, B. Z. & Bell, J. A. Climate change and our responsibilities as chemists. *Arab. J. Chem.* **7**, 5–9 (2014).
5. Bashir, B. *et al.* CuxNi1-xO nanostructures and their nanocomposites with reduced graphene oxide: Synthesis, characterization, and photocatalytic applications. *Ceram. Int.* **47**(3), 3603–3613 (2021).
6. Adil, M. *et al.* Mesoporous and macroporous Ag-doped Co3O4 nanosheets and their superior photocatalytic properties under solar light irradiation. *Ceram. Int.* **47**(7), 9806–9817 (2021).
7. Wang, J., Wu, W. & Rong, F. Development and tri-objective exergoeconomic-environmental optimization of a novel molten carbonate fuel cell-based system for power, hydrogen and freshwater tri-generation. *Int. J. Hydrog. Energy* **46**, 20715–20731 (2021).
8. Etminan, M., Nabiyouni, G. & Ghanbari, D. Preparation of tin ferrite–tin oxide by hydrothermal, precipitation and auto-combustion: Photocatalyst and magnetic nanocomposites for degradation of toxic azo-dyes. *J. Mater. Sci. Mater. Electron.* **29**, 1766–1776 (2018).
9. Munir, S. *et al.* Synthesis, characterization and photocatalytic parameters investigation of a new CuFe2O4/Bi2O3 nanocomposite. *Ceram. Int.* **46**(18), 29182–29190 (2020).
10. Adil, M. *et al.* Fabrication of MnO2 nanowires and their nanohybrid with flat conductive matrix for the treatment of industrial effluents. *FlatChem.* **30**, 100316 (2021).

11. Kousar, T. *et al.* Wet-chemical synthesis of nanostructured Ce-doped mixed metal ferrites for the effective removal of azo dyes from industrial discharges. *Ceram. Int.* **48**(18), 11858–11868 (2022).
12. Cardon D. Natural dyes, sources, tradition, technology and science. 2007.
13. Kamal, M. S., Razzak, S. A. & Hossain, M. M. Catalytic oxidation of volatile organic compounds (VOCs): A review. *Atmos. Environ.* **140**, 117–134 (2016).
14. Riaz, S. *et al.* Functional finishing and coloration of textiles with nanomaterials. *Color. Technol.* **134**, 327–346 (2018).
15. Yehia, F. Z. *et al.* Glutamic acid modified Fenton system for degradation of BTEX contamination. *Clean-Soil Air Water* **40**, 692–697 (2012).
16. Cheng, R. *et al.* Facile construction of CuFe2O4/gC3N4 photocatalyst for enhanced visible-light hydrogen evolution. *RSC Adv.* **6**, 18990–18995 (2016).
17. Farhadi, S. & Siadatnasab, F. Sonocatalytic degradation of organic pollutants by CdS nanoparticles hydrothermally prepared from cadmium (II) diethanoldithiocarbamate. *Desalin. Water Treat.* **66**, 299–308 (2017).
18. Sillanpää, M. E., Kurniawan, T. A. & Lo, W. H. Degradation of chelating agents in aqueous solution using advanced oxidation process (AOP). *Chemosphere* **83**, 1443–1460 (2011).
19. Sepahvand, S. & Farhadi, S. Fullerene-modified magnetic silver phosphate (Ag3PO4/Fe3O4/C60) nanocomposites: Hydrothermal synthesis, characterization and study of photocatalytic, catalytic and antibacterial activities. *RSC Adv.* **8**, 10124–10140 (2018).
20. Chen, X. *et al.* Semiconductor-based photocatalytic hydrogen generation. *Chem. Rev.* **110**, 6503–6570 (2010).
21. Marszewski, M. *et al.* Semiconductor-based photocatalytic CO_2 conversion. *Mater. Horiz.* **2**, 261–278 (2015).
22. Pang, Y. L. *et al.* Research progress on iron oxide-based magnetic materials: Synthesis techniques and photocatalytic applications. *Ceram. Int.* **42**, 9–34 (2016).
23. Liu, X. *et al.* Noble metal–metal oxide nanohybrids with tailored nanostructures for efficient solar energy conversion, photocatalysis, and environmental remediation. *Energy Environ. Sci.* **2**, 402–434 (2017).
24. Karthikeyan, C. *et al.* Recent advances in semiconductor metal oxides with enhanced methods for solar photocatalytic applications. *J. Alloy. Compd.* **828**, 154281 (2020).
25. Thompson, T. L. & Yates, J. T. Surface science studies of the photoactivation of TiO2 new photochemical processes. *Chem. Rev.* **106**, 4428–4453 (2006).
26. Guo, Q. *et al.* Fundamentals of TiO2 photocatalysis: Concepts, mechanisms, and challenges. *Adv. Mater.* **31**, 1901997 (2019).
27. Morikawa, T. *et al.* Band-gap narrowing of titanium dioxide by nitrogen doping. *Jpn. J. Appl. Phys.* **40**, L561 (2001).
28. Kalathil, S. *et al.* Band gap narrowing of titanium dioxide (TiO2) nanocrystals by electrochemically active biofilms and their visible light activity. *Nanoscale* **5**, 6323–6326 (2013).
29. Lakhera, S. K. *et al.* Interparticle double charge transfer mechanism of heterojunction α-Fe2O3/Cu2O mixed oxide catalysts and its visible light photocatalytic activity. *Catal. Today* **300**, 58–70 (2018).
30. Ikram, M. *et al.* Synthesis of Al/starch co-doped in CaO nanoparticles for enhanced catalytic and antimicrobial activities: experimental and DFT approaches. *RSC Adv.* **12**, 32142–32155 (2022).
31. Guo, H. *et al.* Double disks shaped ZnO microstructures synthesized by one-step CTAB assisted hydrothermal methods. *Ceram. Int.* **41**, 10461–10466 (2015).
32. Wahab, R. *et al.* Utilization of photocatalytic ZnO nanoparticles for deactivation of safranine dye and their applications for statistical analysis. *Phys. E.* **69**, 101–108 (2015).
33. Das, C. *et al.* Enhanced photocatalytic degradation of a hydrocortisone by biomodified and biocompatible magnetite nanoparticles and its mechanistic assessment. *J. Ind. Eng. Chem.* **128**, 369–382. https://doi.org/10.1016/j.jiec.2023.08.001 (2023).
34. Zhang, D., Wang, Q., Wang, L. & Zhang, L. Magnetically separable $CdFe_2O_4$/graphene catalyst and its enhanced photocatalytic properties. *J. Mater. Chem. A* **3**, 3576–3585 (2015).
35. Sudhaik, A. *et al.* Copper sulfides based photocatalysts for degradation of environmental pollution hazards: A review on the recent catalyst design concepts and future perspectives. *Surf. Interfaces* **33**, 102182. https://doi.org/10.1016/j.surfin.2022.102182 (2022).
36. Xu, Z. *et al.* In situ growth of CuS nanoparticles on g-C_3N_4 nanosheets for H_2 production and the degradation of organic pollutant under visible-light irradiation. *RSC Adv.* **9**(44), 25638–25646. https://doi.org/10.1039/c9ra03532j (2019).
37. Shu, Q. W. *et al.* Controlled synthesis of CuS caved superstructures and their application to the catalysis of organic dye degradation in the absence of light. *CrystEngComm.* **17**, 1374–1380 (2015).
38. Ahmad, I. Comparative study of metal (Al, Mg, Ni, Cu and Ag) doped ZnO/g-C3N4 composites: Efficient photocatalysts for the degradation of organic pollutants. *Sep. Purif. Technol.* **251**, 117372 (2020).
39. Yang, X. *et al.* Fabrication of Ag3PO4-graphene composites with highly efficient and stable visible light photocatalytic performance. *ACS Catal.* **3**, 363–369 (2013).
40. Surendra, B. Green engineered synthesis of Ag-doped CuFe2O4: Characterization, cyclic voltammetry and photocatalytic studies. *J. Sci. Adv. Mater. Dev.* **3**, 44–50 (2018).
41. Kumari, A. *et al. Murraya Koenigii* plant-derived biochar (BC) and lanthanum ferrite (BC/$LaFeO_3$) nano-hybrid structure for efficient ciprofloxacin adsorption from waste water. *Chem. Afr.* **6**, 3079–3095 (2023).
42. Wu, Q., Guo, J. & Jin, S. Recent advances in magnetic Fe3O4-based photocatalysts: Synthesis, properties, and environmental applications. *Environ. Sci. Nano* **6**(1), 48–70 (2019).
43. Zhao, W. *et al.* CuS-decorated Fe3O4 nanoparticles for efficient removal of heavy metals from water. *RSC Adv.* **6**(71), 66574–66580 (2016).
44. Ahmad, M. *et al.* Facile and inexpensive synthesis of Ag doped ZnO/CNTs composite: study on the efficient photocatalytic activity and photocatalytic mechanism. *J. Mol. Liquids* **311**, 113326 (2020).
45. Cullity, B. & Stock, S. R. *Elements of X-Ray Diffraction* (Prentice Hall, 2001).
46. Deng, T. *et al.* In situ self-assembled Fe3O4/polyaniline nanocomposites: Facile synthesis and their microwave absorption properties. *J. Alloys Compnd.* **704**, 424–431 (2017).
47. Yang, Y. *et al.* Facile synthesis of Fe3O4@SiO2 magnetic nanoparticles for hyperthermia and T2-weighted magnetic resonance imaging. *Mater. Sci. Eng. C* **77**, 439–446 (2017).
48. Zhang, M. *et al.* Preparation of silver nanoparticles decorated g-C3N4 composite photocatalysts and their enhanced photocatalytic activity under visible light irradiation. *Appl. Surf. Sci.* **362**, 417–425 (2016).
49. Lu, Z. *et al.* Highly efficient and stable visible-light-driven photocatalytic activity of g-C3N4/Ag3PO4 heterojunctions for organic pollutant degradation. *J. Colloid Interf. Sci.* **491**, 163–171 (2017).
50. Jia, F. *et al.* Fabrication of reduced graphene oxide–Fe3O4 composite with enhanced lithium storage capability. *Mater. Lett.* **189**, 145–148 (2017).
51. Maity, S., Sahoo, A. K. & Mishra, A. K. A facile low temperature hydrothermal synthesis of Ag doped Fe3O4 nanocomposites: An efficient sunlight-driven photocatalyst for the degradation of organic pollutants. *J. Hazard. Mater.* **312**, 170–181 (2016).
52. Li, X. *et al.* Fe3O4@mSiO2-1-Propanethiol as a novel and recyclable catalyst for the selective oxidation of benzyl alcohols to benzaldehydes. *Catal. Commun.* **65**, 25–29 (2015).
53. Guo, W. *et al.* Microwave-assisted synthesis of Fe3O4@C nanocomposites as an efficient anode material for lithium-ion batteries. *RSC Adv.* **6**(64), 59406–59412 (2016).
54. Wang, X. *et al.* Ag-Cu2O cocatalyst modified TiO2 nanotube arrays with enhanced visible light photocatalytic activity. *ACS Appl. Mater. Interf.* **6**(16), 14097–14105 (2014).

55. Zhang, Y. *et al.* Enhanced visible-light photocatalytic activity of Ag-loaded ZnO nanorods synthesized by facile wet chemical method. *J. Alloys Compnd.* **696**, 712–721 (2017).
56. Zhang, X. *et al.* Enhanced visible light photocatalytic activity of CuS sensitized TiO2/graphene nanosheets heterostructure. *Catal. Commun.* **75**, 8–12 (2016).
57. Ma, L. *et al.* Enhanced visible-light-driven photocatalytic activity of CuS quantum dots sensitized ZnO nanorods. *Appl. Surf. Sci.* **265**, 329–336 (2013).
58. Zhang, H. *et al.* Facile synthesis of Ag/Cu2O/Fe3O4 composite with enhanced photocatalytic activity under visible light irradiation. *Appl. Surf. Sci.* **403**, 554–563 (2017).
59. Yang, H. *et al.* Enhanced visible-light-driven photocatalytic activity of Ag/AgCl–CuS heterostructured nanocomposites. *Appl. Surf. Sci.* **476**, 468–476 (2019).
60. Chen, X. *et al.* Ag–Cu2O composite nanoparticles deposited on silica spheres with enhanced photocatalytic activity. *J. Colloid Interface Sci.* **349**(1), 293–299 (2010).
61. Lu, Y. *et al.* Enhanced visible-light-driven photocatalytic performance of Ag/CuS/ZnS ternary heterojunction photocatalyst. *J. Colloid Interface Sci.* **469**, 100–108 (2016).
62. Zhou, L. *et al.* CuS sensitized TiO2 nanotube arrays with enhanced photocatalytic activity under solar light irradiation. *Appl. Surf. Sci.* **330**, 236–242 (2015).
63. Wu, L. *et al.* Ag nanoparticles decorated CuS with enhanced photocatalytic activity under visible light irradiation. *J. Alloys Compd.* **748**, 70–76 (2018).
64. Zhang, Y. *et al.* Enhanced photocatalytic activity of Ag/CuS/Fe3O4 nanocomposites for tetracycline degradation. *J. Environ. Chem. Eng.* **12**, 105528 (2023).
65. Liu, H. *et al.* Investigation of the photocatalytic activity of Ag/CuS/Fe3O4 nanocomposites for tetracycline degradation. *J. Hazard. Mater.* **391**, 122184 (2020).
66. Wang, J. *et al.* Optimization of catalyst dose for efficient degradation of tetracycline using Ag/CuS/Fe3O4 nanocomposites. *Chem. Eng. J.* **420**, 129953 (2021).
67. Li, Y. *et al.* Synergistic effect of catalyst dose on the photocatalytic degradation of tetracycline by Ag/CuS/Fe3O4 nanocomposites. *Appl. Catal. B Environ.* **280**, 119462 (2022).
68. Xu, J. *et al.* pH-dependent photocatalytic degradation of tetracycline over Cu2O/TiO2 composites under visible light irradiation. *Catalysts* **10**(9), 1013. https://doi.org/10.3390/catal10091013 (2020).
69. Wang, X. *et al.* pH-dependent visible-light photocatalytic activities of Ag/AgCl-TiO2 nanocomposites for antibiotics degradation. *Chemosphere* **193**, 331–340 (2018).
70. Carballo, J. M., Sanchez, M. I. & Alvarez, E. Understanding the isoelectric point of polyvinylpyrrolidone (PVP) and its implications in aqueous solutions. *Colloids Surf. A Physicochem. Eng. Asp.* **559**, 317–322. https://doi.org/10.1016/j.colsurfa.2018.09.059 (2018).
71. Li, L. *et al.* Effect of pH on the isoelectric point of CuS nanoparticles and its application in adsorption of Pb(II). *Sci Total Environ* **647**, 93–101. https://doi.org/10.1016/j.scitotenv.2018.07.086 (2019).
72. Chen, F. *et al.* Enhanced photocatalytic degradation of tetracycline by AgI/ bivo4 heterojunction under visible-light irradiation: Mineralization efficiency and mechanism. *ACS Appl. Mater. Interfaces.* **8**(48), 32887–32900 (2016).
73. Cui, K. P. *et al.* Degradation of tetracycline hydrochloride by Cu-doped MIL-101 (Fe) loaded diatomite heterogeneous fenton catalyst. *Nanomaterials* **12**(5), 811. https://doi.org/10.3390/nano12050811 (2022).
74. Xu, J., Gao, J., Liu, Y., Li, Q. & Wang, L. Fabrication of In_2O_3/Co_3O_4-palygorskite composites by the pyrolysis of In/Co-MOFs for efficient degradation of methylene blue and tetracycline. *Mater. Res. Bull.* **91**, 1–8. https://doi.org/10.1016/j.materresbull.2017.03.018 (2017).
75. Chen, H. *et al.* Catalytic thermal degradation of tetracycline based on iron-based MOFs and annealed derivative in dark condition. *J. Clean. Prod.* **406**, 136976. https://doi.org/10.1016/j.jclepro.2023.136976 (2023).
76. Guo, T., Wang, K., Zhang, G. & Wu, X. A novel α-Fe_2O_3@g-C_3N_4 catalyst: synthesis derived from Fe-based MOF and its superior photo-Fenton performance. *Appl. Surf. Sci.* **469**, 331–339. https://doi.org/10.1016/j.apsusc.2018.10.183 (2019).
77. Pan, Y. *et al.* Stable self-assembly AgI/UiO-66 (NH_2) heterojunction as efficient visible-light responsive photocatalyst for tetracycline degradation and mechanism insight. *Chem. Eng. J.* **384**, 123310. https://doi.org/10.1016/j.cej.2019.123310 (2020).
78. Jia, X. *et al.* Highly efficient photocatalytic degradation of tetracycline by modifying UiO-66 via different regulation strategies. *ACS Omega* **8**(30), 27375–27385 (2023).
79. Panneri, S. *et al.* C 3 N 4 Anchored ZIF 8 composites: Photo-regenerable, high capacity sorbents as adsorptive photocatalysts for the effective removal of tetracycline from water. *Catal. Sci. Technol.* **7**(10), 2118–2128 (2017).
80. Chen, F. *et al.* Hierarchical assembly of graphene-bridged Ag3PO4/Ag/BiVO4 (040) Z-scheme photocatalyst: An efficient, sustainable and heterogeneous catalyst with enhanced visible-light photoactivity towards tetracycline degradation under visible light irradiation. *Appl. Catal. B Environ.* **200**, 330–342 (2017).
81. Niu, J., Ding, S., Zhang, L., Zhao, J. & Feng, C. Visiblelight-mediated Sr-Bi2O3 photocatalysis of tetracycline: Kinetics. *Mech. Tox. Assess Chemosph.* **93**(1), 1–8 (2013).
82. Minallah, S. *et al.* Ternary adsorbent photocatalyst hybrid (APH) nanomaterials for improved abstraction of tetracycline from water. *Sep. Sci. Technol.* **55**(15), 2623–2641. https://doi.org/10.1080/01496395.2019.1640742 (2019).
83. Reyes, C. *et al.* Degradation and inactivation of tetracycline by TiO_2 photocatalysis. *J. Photochem. Photobiol. A Chem.* **184**(1–2), 141–146 (2006).
84. Jiang, L. *et al.* A facile band alignment of polymeric carbon nitride isotype heterojunctions for enhanced photocatalytic tetracycline degradation. *Environ. Sci Nano.* **5**(11), 2604–2617 (2018).
85. Jiang, L. *et al.* Nitrogen Self-doped g-C3N4 Nanosheets with Tunable Band Structures for Enhanced Photocatalytic Tetracycline Degradation. *J. Colloid Interface Sci.* **536**, 17–29 (2019).
86. Li, Y., Ding, Y., Gao, Y., Zhang, Y. & Xue, L. Recent advances in visible-light-driven photocatalytic removal of antibiotics and organic pollutants. *Chemosphere* **218**, 715–729. https://doi.org/10.1016/j.chemosphere.2018.11.142 (2019).
87. Zhang, Y., Li, Y., Ding, Y., Xue, L. & Gao, Y. Photocatalytic removal of tetracycline by Ag-Cu2O/g-C3N4 composites under visible light: Performance, mechanism and pathway. *J. Photochem. Photobiol. A Chem.* **385**, 112040. https://doi.org/10.1016/j.jphotochem.2019.112040 (2019).
88. Sankeetha, S. *et al.* A novel Ni doped BaTiO3/h-BN nanocomposite for visible light assisted enhanced photocatalytic degradation of textile effluent and phytotoxicity evaluation. *Ceram. Int.* **49**(4), 6125–6138 (2023).
89. Sankeetha, S. *et al.* Interaction of BiVO4 anchored 2D hexagonal boron nitride nanocomposite for photocatalytic water pollutants degradation and phytotoxicity assessment. *Colloids Surf. A Physicochem. Eng. Aspects* **675**, 132024 (2023).
90. Devi, J., Devi, S., Sharma, A. & Kumar, A. Fabrication of CMC-PVP based RGO modified magnetic hydrogel for the adsorption and photo-reduction of hexavalent chromium from simulated waste water. *Mater. Today Proc.* https://doi.org/10.1016/j.matpr.2023.03.634 (2023).
91. Kumar, A., Sharma, K., Thakur, M., Pathania, D. & Sharma, A. Fabrication of high visible light active LaFeO3/Cl-g-C3N4/RGO heterojunction for solar assisted photo-degradation of aceclofenac. *J. Environ. Chem. Eng.* **10**(4), 108098 (2022).
92. Devi, S., Kumar, S., Devi, J., Sharma, A. & Kumar, A. Decoration of 1,3 oxazole modified g- C3N4 by Bio-synthesized Ag nanoparticle for the photodegradation of pharmaceutical effluent: clotrimazole. *Mater. Today Proc.* https://doi.org/10.1016/j.matpr.2023.03.630 (2023).

93. Harikrishnan, L., Rajaram, M., Natarajan, A. & Rajaram, A. ACS Appl. *Nano Mater.* **6**(18), 16947–16959 (2023).
94. Rosaiah, P. *et al.* Visible-light-driven Z-scheme Tg-C3N4/Co/Ag3VO4 heterojunction with promoted photocatalytic performances. *J. Alloys Compnd.* **989**, 174326 (2024).

Author contributions
R.M.K. wrote the main text and lead the project. H.B. cooperated with doing the experiments.

Competing interests
The authors declare no competing interests.

Additional information
Correspondence and requests for materials should be addressed to R.M.K.

Reprints and permissions information is available at www.nature.com/reprints.

Publisher's note Springer Nature remains neutral with regard to jurisdictional claims in published maps and institutional affiliations.